Impact of crystallinity on enzyme orientation and dynamics upon biomineralization in Metal-Organic Frameworks (MOFs)

Zoe Armstrong,[#,1] Austin MacRae,[#,1] Mary Lenertz, [1] Qiaobin Li, [1] Kelley Johnson,[1] Allison Scheiwiller,[1] Patrick Shen,[2] Li Feng,[1] Mohiuddin Quadir,[3] and Zhongyu Yang*[,1]

1. Department of Chemistry and Biochemistry, North Dakota State University, Fargo, North Dakota, 58102 U.S.A

2. Davis High School, Fargo, North Dakota 58104 U.S.A

3. Department of Coatings and Polymeric Materials, North Dakota State University, Fargo, North Dakota 58102 U.S.A

#These authors contribute equally to this work

Corresponding to: zhongyu.yang@ndsu.edu

Keywords: Metal-Organic Frameworks (MOFs), Enzyme encapsulation, Enzyme orientation, Site-direct spin labeling (SDSL), Electron Paramagnetic Resonance (EPR)

Abstract

Aqueous-phase co-crystallization (also known as biomimetic mineralization or biomineralization) is a unique way to encapsulate large enzymes, enzyme clusters, and enzymes with large substrates in Metal-Organic Frameworks (MOFs), broadening the application of MOFs as enzyme carriers. The crystallinity of resultant enzyme@MOF biocomposites, however, can be low, raising a concern on how MOF crystal packing quality affects enzyme performance upon encapsulation. The challenges to overcome this concern are: 1) the limited data base of enzyme performance upon biomineralization in different aqueous-MOFs and 2) the difficulty in probing enzyme restriction and motion in the resultant MOF scaffolds, which are related to the local crystal packing quality/density, under the interference of the MOF backgrounds. We have discovered several new aqueous-MOFs for enzyme biomineralization with varied crystallinity [*ACS App. Mater. Interfaces 2022, 14, 51619-51629*]. Here, we address the second challenge by probing enzyme dynamics/restriction in these MOFs at the residue level via site-directed spin labeling (SDSL) – Electron Paramagnetic Resonance (EPR) spectroscopy, a unique approach to determine protein backbone motions regardless of the background complexity. We encapsulated a model large-substrate enzyme, lysozyme, in 8 newly discovered MOFs, which possess varied degree of crystallization, via aqueous phase co-crystallization. Through EPR study and simulations, we found rough connections between a) enzyme mobility/dynamics and MOF crystal properties (packing quality and density) and b) the enzyme areas exposed above each MOF and their catalytic performance. This work suggests that protein SDSL and EPR can serve as an indicator of MOF crystal packing quality/density when biomineralized in MOFs. The method can be generalized to probing the dynamics of other enzymes on other solid surfaces/interfaces and guide the rational design of solid platforms (ca. MOFs) to customize enzyme immobilization.

Introduction

Metal-Organic Frameworks (MOFs) are advanced platforms for enzyme encapsulation and the cell-free investigation of enzyme biophysics under spatial confinement.[1-17] The sizes of enzymes and substrates are often smaller than MOF pores/apertures to allow sufficient diffusion. For larger enzymes and enzyme clusters, co-crystallization can be applied which exposes a small portion of an enzyme above the crystal surface, allowing large substrates (with respect to MOF pores) to be catalyzed.[13, 18-29] The reaction medium of co-crystallization is often an organic solvent to enhance the crystallinity, which limits this approach to relatively stable enzymes with certain protection.[18, 30] Aqueous-phase co-crystallization of enzymes with metal ions and ligands recently explored by us and other research teams removes this limitation.[23, 30-35] Two practical drawbacks, however, are 1) the sacrifice of crystallinity, which may also explain why this approach is less popular in enzyme encapsulation, and 2) the instability of the formed enzyme@MOF composites which, on the other hand, can be used for enzyme release.[20]

The former often leads to questions on how MOF crystal packing quality influences enzyme dynamics/function and how enzyme mobility is connected to/dependent on MOF crystallinity. Establishing such connections is important for understanding the performance of enzymes in the MOF scaffolds and building a database for the rational selection of metal ions and ligands, and thus, crystallinity, to tune enzyme performance in MOFs via biomineralization. Obtaining this information, however, is challenging due to 1) the lack of available MOFs to encapsulate enzymes via biomineralization, 2) the interference of the MOF background and the heterogeneity in enzyme orientation and dynamics, and 3) the difficulty in detecting the subtle differences in enzyme dynamics in MOFs differing in crystallinity for most protein-probing techniques. We recently discovered several new combinations of metal ions and ligands to

biomineralize enzymes in water with varied degree of crystallinity and packing quality.[35] We have also developed an experimental strategy to probe enzyme backbone dynamics in MOFs via site-directed spin labeling (SDSL) – Electron Paramagnetic Resonance (EPR) spectroscopy and tested it in other MOFs.[36-37] SDSL-EPR probes enzyme dynamics and structural information at the residue level regardless of the complexities caused by the background and heterogeneity.[38-42] EPR is sensitive to protein backbone dynamics on ~ns order,[43-44] which can rapidly report if a labeled site is in contact with MOF crystal scaffolds or not; in the former case, EPR can also detect the subtle differences in enzyme backbone dynamics caused by differences in MOF crystallinity.[31, 36] In a heterogeneous condition, EPR detects all contributions from different components; spectral simulation can then deconvolute the contribution of each. Doing so on multiple surface sites of the target enzyme can reveal the average motional restriction an enzyme experiences in a MOF and areas of enzyme exposed above the surface of a MOF.[45] Meanwhile, the exposed area and backbone dynamics of enzymes are indicators of MOF crystal property.

In this work, for proof-of principle, we apply this strategy to reveal the orientation and dynamics of a model large-substrate enzyme, T4 phage lysozyme (T4L), upon encapsulations in 8 MOFs via biomineralization.[35] These MOFs possess varied degree of crystallization (single-crystals, multi-phase crystals, and amorphous, gel-like crystals) based on the combination of 4 metal ions and 2 ligands. We found that the restriction in the motional dynamics of the labeled sites on the surface of T4L increases as the packing quality/density is increased. Also, we revealed the exposed areas of the entrapped protein above the surface of each MOF crystal, which is roughly consistent with the catalytic performance of the model large-substrate enzyme, T4L. This work not only demonstrates the established strategy for probing enzyme orientation and dynamics upon biomineralization in MOFs but also offers a molecular "indicator" to probe MOF properties. The

strategy can be generalized to probing the orientation and dynamics of other enzymes on other solid surfaces and guide the rational design of solid platforms (ca. MOFs) to customize the enzyme immobilization.

Results and Discussion

Experimental design. The co-crystallization procedures of our model enzyme, T4 phage lysozyme (T4L), with 4 metal ions, Zn^{2+}, Ni^{2+}, Al^{3+}, and Zr^{4+}, and 2 ligands, terephthalate sodium (BDC−Na_2) and biphenyl-4,4-dicarboxylate sodium (BPDC−Na_2),[46-52] published in our recent work are directly applied here to prepare samples in this work.[35] T4L is selected because of its large substrates (bacterial cell walls) which require partial enzyme exposure to delivery its biocatalytic function.[35, 53-54] The MOFs are selected due to their difference in crystallinity: single crystal (Zn-BDC/BPDC), multi-phase crystals (Ni-BDC/BPDC and Al-BDC/BPDC), and amorphous crystals (Zr-BDC/BPDC).[55-58] To probe the enzyme's contact with MOF scaffold and expose above MOF crystals, we selected eight surface sites of T4L to cover most of the protein regions (Figure 1A), mutated each to a cysteine, one at a time, and spin labeled each with a nitroxide spin label (Figure 1B). Details are provided in the Supporting Information and our recent work (SI).[59] Each mutant was then co-crystallized in each of the eight MOFs, followed by CW EPR studies using published protocols. The raw data of all 64 spectra are shown in the SI (Figures S1-S4). To analyze these data, CW EPR spectral simulation based on established algorithms and software were carried out.[37, 60] Details of simulation method and representative simulation result are presented in the SI (Tables S1-S8 and Figure S5; example fitting is shown in Figure S6). Here we summarize the strategies employed in this work when analyzing the results from our simulations.

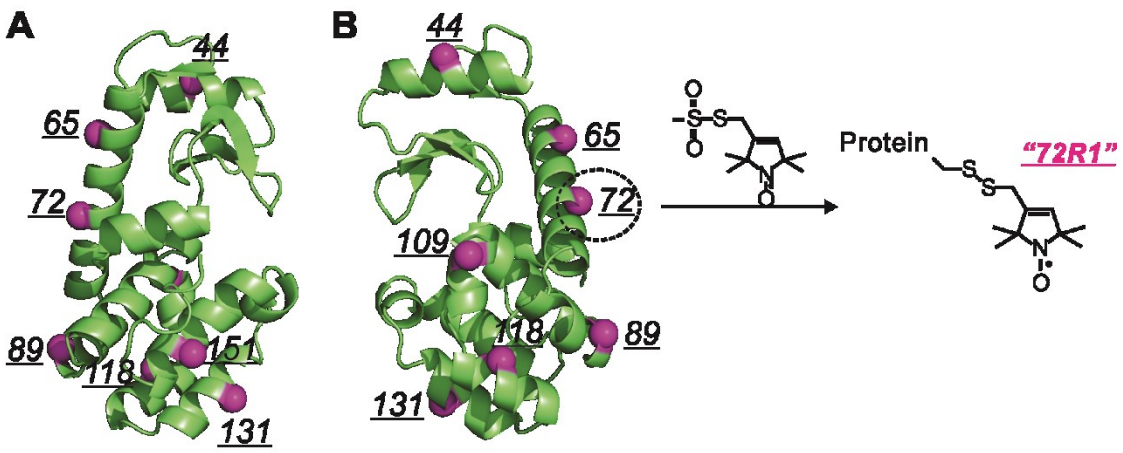

Figure 1. (A) Eight surface sites of the model enzyme, T4L, involved in this work. (B) Schematic illustration of SDSL of a representative site, 72C to generate a spin label sidechain (named as "D72C-R1").

The key simulation results include: 1) the relative population of the "mobile" and "immobile" components originated from exposed and contact/restricted labeled sites, respectively, 2) the rates characterizing protein backbone motion, and 3) the relative spaces available/allowed for the motion (order parameter) of each component. Although the population was often used to depict the exposed area of an enzyme entrapped in a MOF to explain the catalytic activity in most works,[30-31, 33-34] in this work we will also explore the correlation between enzyme mobility and crystallinity. First, the average rate of the "mobile" components for all labeled sites serves as an indicator of the overall mobility of the protein above a MOF surface. Comparing the average "mobile" rate among all MOFs will then result in the relative mobility of the portions of the enzyme exposed above all MOFs, which will report MOF crystal quality because a MOF with low crystallinity or loose packing could place less restriction on the "anchor" of the protein (Figure 2A).

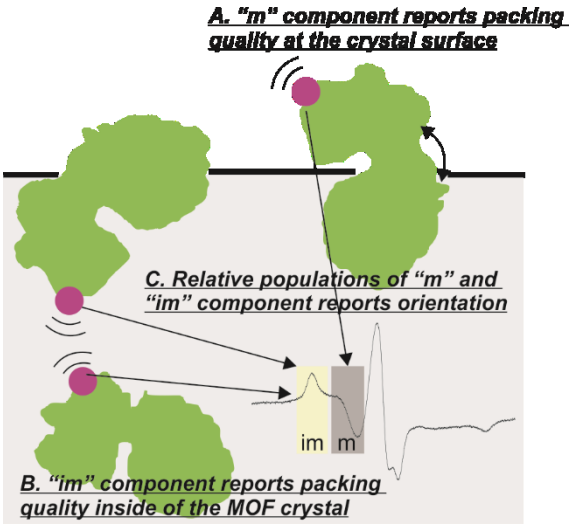

Figure 2. Schematic illustration of the key structural information from an EPR spectrum of a labeled protein and its sensitivity to crystal properties. Definitions of the "m" and "im" components see the main text. (A) Illustration of the case where the "m" spectral component reports packing quality at the crystal surface. (B) Illustration of the case where the "im" spectral component reflects packing quality inside of the MOF crystal. (C) Schematic illustration of the case where the relative populations of the "m" and "im" components pinpoint the enzyme orientation.

Next, to probe protein mobility and crystal packing quality inside of a MOF, we will focus on the average rate of the "immobile" component of all labeled sites. The "immobile" component is caused by a labeled site contacting the MOF scaffold, which creates restriction on protein mobility and also depends on the crystallinity and packing density (the tighter the packing, the lower the protein mobility; Figure 2B). Thus, the average rates of the "immobile" and "mobile" components of all labeled site covering most of the protein surface are indicators of the overall crystallinity and packing quality of the MOF.

Finally, focusing on one MOF, the population difference between the "immobile" and "mobile" components tells the chance for a labeled site to be exposed (Figure 2C). Scanning all labeled sites will reveal the areas (sites) with a higher chance to be exposed above MOF surface, and thus, enzyme orientation on MOF surface. Below we will sequentially discuss the effects of MOF crystallinity, linker, and metal ions on all simulation parameters and thus, enzyme orientation and dynamics via EPR and simulation.

Packing quality and density inside of the MOF crystals. The motion of a spin labeled sidechain buried inside of a MOF crystal depends on the restrictions of the sidechain motion, which further depend on how tightly the scaffold is packed at the labeled site. Although different sites of a protein within a MOF scaffold could face different extents of restriction, the overall restriction to a buried protein, or, the average of the motion of the "im" component, should reflect the overall packing inside of a MOF. Bearing this in mind, we found that for the same ligand (ca. BDC), the average rates (definition see the SI; usually the higher the rate parameter, the faster the motion, and the less restriction in motion) of the "im" over 8 labeled T4L sites in the four MOFs are ~6.00 (Zn-BDC), ~6.01 (Ni-BDC), ~6.03 (Al-BDC), and ~6.06 (Zr-BDC; Table 1). Although the difference seems to be subtle, the trend follows a decrease in crystallinity (see Figure 3; Zn-BDC: single crystal → Ni-BDC: multiphase crystal → Al-BDC: multiphase crystal with lower crystallinity → Zr-BDC: amorphous crystal, gel-like).[35] The subtle differences suggest that the loss in crystallinity is not significant. For MOFs formed by BPDC, the differences in the rate of the "im" component are more significant: ~5.89 (Zn-BPDC), ~5.91 (Ni-BPDC), ~5.95 (Al-BPDC), and ~6.15 (Zr-BPDC), also follows the same trend of decrease in crystallinity (see Figure 3; Zn-BPDC: single crystal → Ni-BPDC: multiphase crystal → Al-BPDC: multiphase crystal with low crystallinity → Zr-BPDC:

amorphous crystal, gel-like). Thus, the motion of spin labeled protein sidechains is sensitive to and reflects the packing quality/density of aqueous-phase MOFs (Figure 3).

Table 1. Average rates of the "m" and "im" components over all 8 labeled sites of T4L on each involved MOF in this work. The higher the rate parameter, the faster the motion, and the less restriction in motion

	Zn-BDC	Zn-BPDC	Ni-BDC	Ni-BPDC	Al-BDC	Al-BPDC	Zr-BDC	Zr-BPDC
R_{im}	6.00	5.89	6.01	5.91	5.98	5.95	6.06	6.15
R_m	8.16	7.64	8.01	7.86	8.11	8.09	7.94	8.09

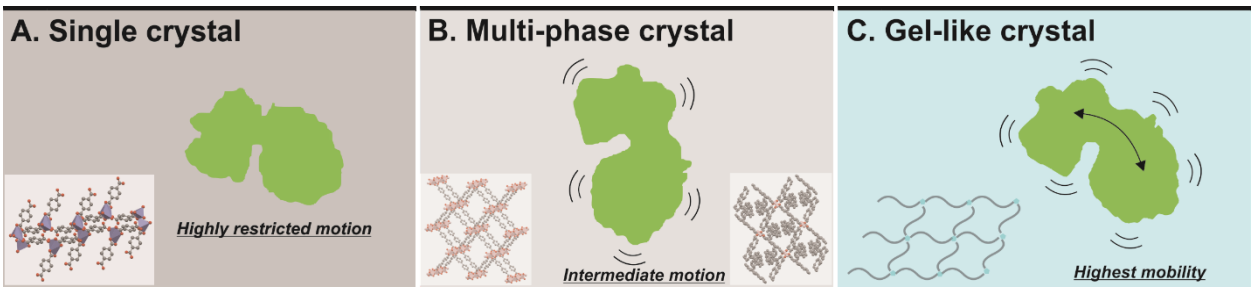

Figure 3. Schematic illustration of correlation between crystal packing quality and enzyme mobility upon encapsulation in a single-crystal MOF (A), multi-phase MOF (B), and gel-like amorphous MOF (C).

Effects of the ligand. An interesting finding is that the longer ligand, BPDC, did not necessarily result in larger gaps and thus, enhanced motion in the "im" component. Instead, for the 3 out of the 4 studied metal ions (Zn^{2+}, Ni^{2+}, and Al^{3+}), the rate of the "im" component is lower as compared to that in the MOF formed with BDC (Table 1; 5.89 vs 6.00, 5.91 vs 6.01, and 5.95 vs 6.03 for Zn^{2+}, Ni^{2+}, and Al^{3+}, respectively). This is not a surprise because the packing density is not

necessarily proportional to the ligand size. The crystals of the MOFs formed by BPDC and Zn^{2+}, Ni^{2+}, and Al^{3+} display a layer-by-layer, 2-dimentional (2D) structures which would allow less space if a protein is trapped.[35] In fact, these 2D materials should be more accurately named as Metal-Organic Materials (MOMs) instead of MOFs; MOFs are often considered to be 3D structures formed by the frameworks of metal ions and ligands.[35] In our case, most likely the 2D, layer-by-layer packing is more intense than the 3D cases. Note that the difference between Al-BPDC and Al-BDC is small, which may be caused by the fact that Al-BDC seems to be close to a layered structure as well.[35] The rate of the "im" component of in Zr-BPDC, however, is faster than that in Zr-BDC (6.15 vs 6.06). This is rationalized to the poor crystallinity so that the Zr-based MOFs are more like gels formed by crosslinked linkers and joints (Figure 3C). The longer the linker, the more spaces for a trapped protein and thus, the fast the rate of motion. Once again, the sensitivity of CW EPR to the local motion of a protein trapped in a MOF/MOM/gel can report the packing quality/density of the material.

Probing the interface of "trapping". Although the "m" component is originated from the portion of a protein exposed above the MOF crystal surface and can vary depending on labeled site, its rate is also related to the packing of the MOF crystal. For example, in a tightly packed, layer-by-layer Zn-BPDC, the motion of the exposed portion of the protein is also more restricted as compared to the less intensely packed Zn-BDC (7.64 vs 8.06; Table 1), likely due to the less wiggling room at the interface of protein and Zn-BPDC (Figure 2A). The detected rate of the "m" component depends on not only the nearby substances (which may contact the labeled site) but also the summation of protein tumbling, backbone motion, and spin label's intrinsic motion; the less the wiggling at the interface, the less protein tumbling, and thus, the slower the rate of the resultant "m" component's motion. The same trend is true for Ni-BPDC and Ni-BDC (7.86 vs

8.01) as well as Al-BPDC and Al-BDC (8.09 vs 8.11), although the difference between Al-BPDC and Al-BDC is small, which is also consistent with their close packing style (Al-BDC seems to be close to a layered structure as well).[35] For Zr-based MOFs, the rate of the "m" component is faster in Zr-BPDC as compared to that in Zr-BDC (8.09 vs 7.94), also consistent with the higher gaps and longer linker in the former in a gel-like material.

Exposed areas of the trapped enzyme. The relative population of the "m" component is a direct reflection of the chance for a labeled site to be exposed above a MOF crystal surface. Scanning multiple surface regions of a target protein will result in the preference of protein regions being exposed above MOF crystals. Taking Zn-BDC as an example, the difference among different labeled sites in the percentage of the "m" component is small (all ~50%; Table S1), indicating that the trapping is really a random process with almost equal preference for all protein regions to be exposed. There are no preferred regions of T4L being exposed (Figure 4A). Note that the active site of T4L in/near the N-terminus of the protein, which may be related to the catalytic activity against a large substrate. Zn-BPDC, on the other hand, shows a favorable exposure region of C-terminal 44 (50.0%) and 109 (65.4%), followed by 151 (>40%) as compared to the (near 30%) chance of exposure of all other labeled sites. Thus, a proposed T4L orientation on Zn-BPDC is shown in Figure 4B. The catalytic activities of T4L in the two Zn-based MOFs are close, consistent with the similar chance of exposing the N-terminus (Figure 4C).

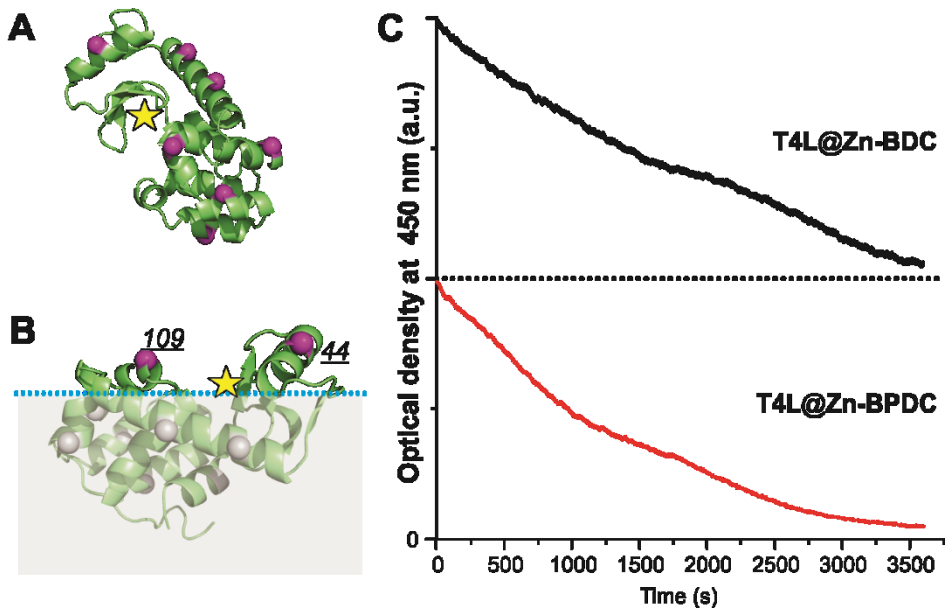

Figure 4. The exposed regions of T4L upon encapsulation in Zn-BDC and Zn-BPDC biocomposites and the associated catalytic performance. (A) On Zn-BDC, all labeled sites have similar opportunities to be exposed so that no preferred orientation or exposed regions are specified. (B) On Zn-BPDC, only 44 and 109 show a higher chance of being exposed, based on which a preferred orientation is proposed. (C) The drops in optical density at 450 nm, especially the slopes at the beginning region, in the activity assay of T4L on Zn-BDC and Zn-BPDC suggest a close catalytic efficiency between these two biocomposites, which can be rationalized to the similar extent of exposing the active site (yellow star) above the MOF crystal surface.

For Ni-BDC, the C-terminus, 151 shows the highest chance to be exposed (45.7%), while the N-terminus representatives (44, 65, and 72) are exposed less (32.2, 42.2, and 20.1 %; Figure 5A). On Ni-BPDC, the N-terminal 44 (45.0%), 72 (35.1%), and 89 (54.9 %) regions are more likely to be exposed (Figure 5B). T4L activity on Ni-BPDC is slightly higher than that on Ni-BDC

(Figure 5C; activity is approximately proportional to the slope),[35] consistent with the chance of exposing the N-terminus.

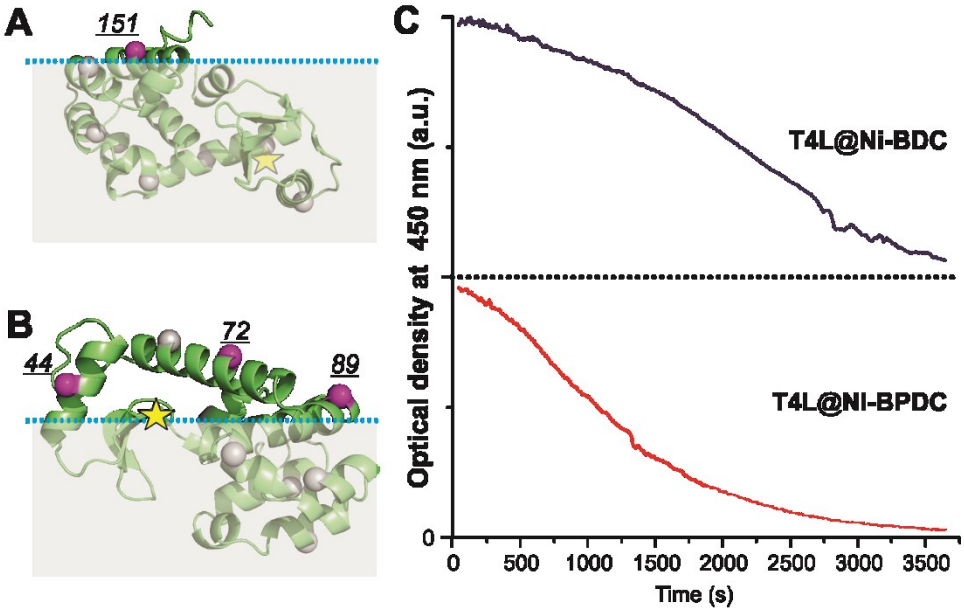

Figure 5. The exposed regions of T4L upon encapsulation in Ni-BDC and Ni-BPDC biocomposites and the associated catalytic performance. (A) On Ni-BDC, the C-terminus representative, T151C-R1, has the highest chance to be exposed, based on which a preferred orientation is proposed. (B) On Ni-BPDC, the N-terminus representatives, S44C-R1, D72C-R1, and D89C-R1 show a higher chance of being exposed, based on which a preferred orientation is proposed. (C) The drops in optical density at 450 nm, especially the slopes at the beginning region, in the activity assay of T4L on Ni-BDC and Ni-BPDC suggest a higher catalytic efficiency in T4L@Ni-BPDC as compared to that in T4L@Ni-BDC, which can be rationalized to the slightly higher extent of exposing the active site (yellow star) in the former.

On Al-BDC, the most favored region to be exposed is 118/131 areas (48.8 and 48.9%; Figure 6A), while the N-terminal 44 and 65 are exposed in a much lower chance (35.3 and 34.7%).

On Al-BPDC, many residues are exposed with more than 55% chance including both the N-terminus (S44C-R1: 58.2%; K65C-R1: 57.3%; D72C-R1: 53.3%) and the C-terminus (V131C-R1: 57.2%; T151C-R1: 48.9%; Figure 6B). The catalytic activity of T4L in Al-BPDC is also higher than that in Al-BDC (Figure 6C), consistent with the chance of exposing the N-terminus.

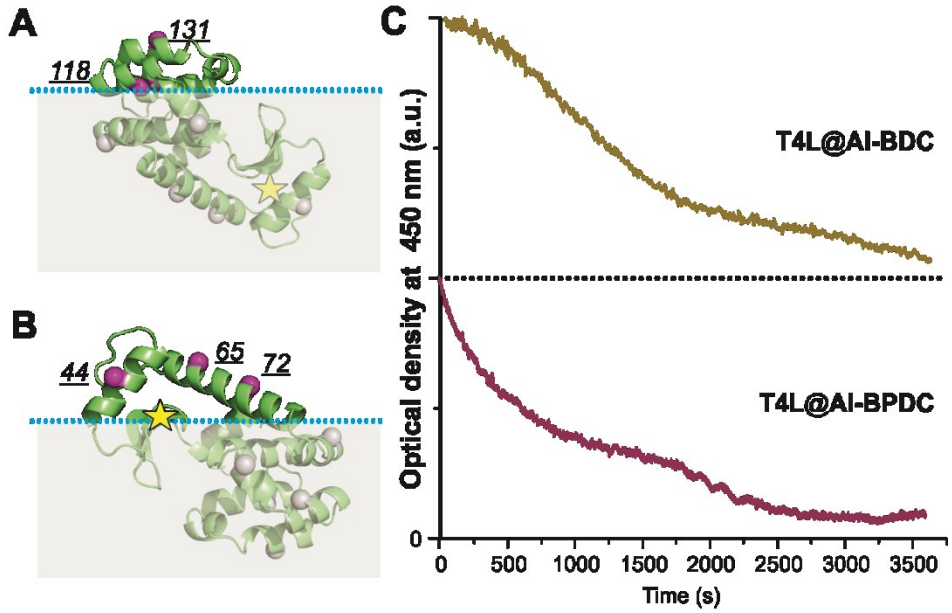

Figure 6. The exposed regions of T4L upon encapsulation in Al-BDC and Al-BPDC biocomposites and the associated catalytic performance. (A) On Al-BDC, the C-terminus representatives, L118C-R1 and V131C-R1, have the highest chance to be exposed, based on which a preferred orientation is proposed. (B) On Al-BPDC, the N-terminus representatives, S44C-R1, K65C-R1, and D72C-R1 show a higher chance of being exposed, based on which a preferred orientation is proposed. (C) The drops in optical density at 450 nm, especially the slopes at the beginning region, in the activity assay of T4L on Al-BDC and Al-BPDC suggest a higher catalytic efficiency in T4L@Al-BPDC as compared to that in T4L@Al-BDC, which can be rationalized to the slightly higher extent of exposing the active site (yellow star) in the former.

On the gel-like Zr-BDC, both the N-terminus (S44C-R1: 46.0%; K65C-R1: 60.9%) and the C-terminus (T151C-R1: 59.1%) as well as 118 region tend to be exposed. On Zr-BPDC, most residues are exposed ≥50 % including the N-terminus (S44C-R1: 58.9%; K65C-R1: 57.6%; D72C-R1: 54.3%), the C-terminus (T151C-R1:49.7%), and the 89/109 region (69.8% and 56.1%). Taken together, EPR data offer an opportunity to probe the chance of a trapped protein on a MOF surface and thus, the chance to contact substrates larger than MOF pores. Note that the catalytic activity of T4L in these MOFs is not necessarily proportional to the percentage of exposing the N-terminus, because other factors such as particle size of the MOF, surface charge, and surface hydrophobicity may also influence the detected activity. However, the trend of activity when comparing T4L in MOFs formed by the same metal ion seems to match the chance of exposing the N-terminus.

Conclusion

This work shows an approach to investigate the interface of proteins/enzymes upon encapsulation in MOFs via biomineralization at the resolution of molecular to residue level. The key to do so is to combine SDSL of enzyme with EPR spectroscopy, which probes the dynamics and order of protein sidechain motion at the residue level regardless of the complexity caused by the MOF background. We found a rough connection between protein mobility/dynamics and MOF crystal properties (packing quality and density). In particular, the restriction in the motional dynamics of 8 labeled sites on the surface of a model protein increases as the packing quality/density is increased when different metal ions are employed (gel-like amorphous crystals → multi-phase crystals → single crystals). For the same metal ion, the ligand affects the packing and motional dynamics of the labeled sidechain as well, so that BPDC which creates intensely packed, layer-by-layer 2D MOMs results in higher restriction in the motion of the trapped protein as compared to the 3D MOF crystals. However, when forming gel-like materials, the longer ligand BPDC results

in less restriction in protein motion than the shorter BDC does. Furthermore, we revealed the exposed areas and extent of active site exposure of the entrapped enzyme above the surface of each MOF crystal, which is roughly consistent with the catalytic performance of the model large-substrate enzyme, T4L. This work indicates the power of SDSL-EPR in probing protein dynamics in complex environments; the resultant findings not only lead to the rationalization of enzyme function upon biomineralization but also serve as indicators of the packing quality of the MOF crystals. This approach can be applied to other MOFs or packing platforms to immobilize enzymes.

Supporting information

Additional experimental details and data analysis procedures, including protein spin labeling approaches, simulation principles and procedures, protein activity assays, raw data of all involved EPR spectra, representative simulation results, and simulation parameters to fit each spectrum (64 total).

Supporting information is available free of charge at xxx.

Notes

The authors declare no competing financial interest.

Acknowledgements

This work is supported by the National Science Foundation (NSF, MCB 1942596 to Z.Y.). The authors appreciate Dr. Piotr Fajer for generously donating the Bruker EMX EPR spectrometer to Z.Y.'s research group.

References

1. Wang, X.; Lan, P. C.; Ma, S., Metal-Organic Frameworks for Enzyme Immobilization: Beyond Host Matrix Materials. *ACS Centr. Sci.* **2020,** *6*, 1497-1506.
2. Lian, X.; Fang, Y.; Joseph, E.; Wang, Q.; Li, J.; Banerjee, S.; Lollar, C.; Wang, X.; Zhou, H.-C., Enzyme-MOF (Metal-Organic Framework) Composites. *Chem. Soc. Rev.* **2017,** *46* (11), 3386-3401.
3. Drout, R. J.; Robison, L.; Farha, O. K., Catalytic Applications of Enzymes Encapsulated in Metal-Organic Frameworks. *Coord. Chem. Rev.* **2019,** *381*, 151-160.
4. Majewski, M. B.; Howarth, A. J.; Li, P.; Wasielewski, M. R.; Hupp, J. T.; Farha, O. K., Enzyme Encapsulation in Metal-Organic Frameworks for Applications in Catalysis. *CrystEngComm* **2017,** *19* (29), 4082-4091.
5. Howarth, A. J.; Liu, Y.; Li, P.; Li, Z.; Wang, T. C.; Hupp, J. T.; Farha, O. K., Chemical, Thermal and Mechanical Stabilities of Metal-Organic Frameworks. *Nat. Rev. Mater.* **2016,** *1*, 15018.
6. Gkaniatsou, E.; Sicard, C. m.; Ricoux, R. m.; Mahy, J.-P.; Steunou, N.; Serre, C., Metal-Organic Frameworks: A Novel Host Platform for Enzymatic Catalysis and Detection. *Mater. Horiz.* **2017,** *4* (1), 55-63.
7. Fang, Y.; Powell, J. A.; Li, E.; Wang, Q.; Perry, Z.; Kirchon, A.; Yang, X.; Xiao, Z.; Zhu, C.; Zhang, L.; Huang, F.; Zhou, H.-C., Catalytic Reactions within the Cavity of Coordination Cages. *Chem. Soc. Rev.* **2019,** *48* (17), 4707-4730.
8. Mehta, J.; Bhardwaj, N.; Bhardwaj, S. K.; Kim, K. H.; Deep, A., Recent Advances in Enzyme Immobilization Techniques: Metal-Organic Frameworks as Novel Substrates. *Coord. Chem. Rev.* **2016,** *322*, 30-40.
9. Liang, J.; Gao, S.; Liu, J.; Zulkifli, M. Y. B.; Xu, J.; Scott, J.; Chen, V.; Shi, J.; Rawal, A.; Liang, K., Hierarchically Porous Biocatalytic MOF Microreactor as a Versatile Platform towards Enhanced Multienzyme and Cofactor-Dependent Biocatalysis. *Angew. Chem. Inter. Ed.* **2021,** *60* (10), 5421-5428.
10. Hu, C.; Bai, Y.; Hou, M.; Wang, Y.; Wang, L.; Cao, X.; Chan, C.-W.; Sun, H.; Li, W.; Ge, J.; Ren, K., Defect-Induced Activity Enhancement of Enzyme-Encapsulated Metal-Organic Frameworks Revealed in Microfluidic Gradient Mixing Synthesis. *Sci. Adv.* **2020,** *6* (5), eaax5785.
11. Tian, D.; Zhang, X.; Shi, H.; Liang, L.; Xue, N.; Wang, J.-H.; Yang, H., Pickering-Droplet-Derived MOF Microreactors for Continuous-Flow Biocatalysis with Size Selectivity. *J. Am. Chem. Soc.* **2021,** *143* (40), 16641-16652.
12. Man, T.; Xu, C.; Liu, X.-Y.; Li, D.; Tsung, C.-K.; Pei, H.; Wan, Y.; Li, L., Hierarchically encapsulating enzymes with multi-shelled metal-organic frameworks for tandem biocatalytic reactions. *Nat. Commun.* **2022,** *13* (1), 305.
13. Li, Y.-M.; Yuan, J.; Ren, H.; Ji, C.-Y.; Tao, Y.; Wu, Y.; Chou, L.-Y.; Zhang, Y.-B.; Cheng, L., Fine-Tuning the Micro-Environment to Optimize the Catalytic Activity of Enzymes Immobilized in Multivariate Metal–Organic Frameworks. *J. Am. Chem. Soc.* **2021,** *143* (37), 15378-15390.
14. Du, Y.; Jia, X.; Zhong, L.; Jiao, Y.; Zhang, Z.; Wang, Z.; Feng, Y.; Bilal, M.; Cui, J.; Jia, S., Metal-organic frameworks with different dimensionalities: An ideal host platform for enzyme@MOF composites. *Coordination Chemistry Reviews* **2022,** *454*, 214327.

15. Liang, W.; Wied, P.; Carraro, F.; Sumby, C. J.; Nidetzky, B.; Tsung, C.-K.; Falcaro, P.; Doonan, C. J., Metal–Organic Framework-Based Enzyme Biocomposites. *Chemical Reviews* **2021,** *121* (3), 1077-1129.
16. Chen, W.-H.; Vázquez-González, M.; Zoabi, A.; Abu-Reziq, R.; Willner, I., Biocatalytic cascades driven by enzymes encapsulated in metal–organic framework nanoparticles. *Nature Catalysis* **2018,** *1* (9), 689-695.
17. Zhang, Y.; Xu, L.; Ge, J., Multienzyme System in Amorphous Metal–Organic Frameworks for Intracellular Lactate Detection. *Nano Letters* **2022,** *22* (12), 5029-5036.
18. Lyu, F.; Zhang, Y.; Zare, R. N.; Ge, J.; Liu, Z., One-Pot Synthesis of Protein-Embedded-Supporting Information. *Nano Letters* **2014,** *14* (10), 5761-5765.
19. Liang, W.; Xu, H.; Carraro, F.; Maddigan, N. K.; Li, Q.; Bell, S. G.; Huang, D. M.; Tarzia, A.; Solomon, M. B.; Amenitsch, H.; Vaccari, L.; Sumby, C. J.; Falcaro, P.; Doonan, C. J., Enhanced Activity of Enzymes Encapsulated in Hydrophilic Metal-Organic Frameworks. *J. Am. Chem. Soc.* **2019,** *141* (6), 2348-2355.
20. An, H.; Song, J.; Wang, T.; Xiao, N.; Zhang, Z.; Cheng, P.; Huang, H.; Ma, S.; Chen, Y., Metal-Organic Framework Disintegrants: A New Generation of Enzyme Preparation Platforms with Boosted Activity. *Angew. Chem. Inter. Ed.* **2020,** *59* (10.1002/anie.202007827), 16764-16769.
21. Saliba, D.; Ammar, M.; Rammal, M.; Al-Ghoul, M.; Hmadeh, M., Crystal Growth of ZIF-8, ZIF-67, and Their Mixed-Metal Derivatives. *J. Am. Chem. Soc.* **2018,** *140* (5), 1812-1823.
22. Cravillon, J.; Schröder, C. A.; Nayuk, R.; Gummel, J.; Huber, K.; Wiebcke, M., Fast Nucleation and Growth of ZIF-8 Nanocrystals Monitored by Time-Resolved In Situ Small-Angle and Wide-Angle X-Ray Scattering. *Angew. Chem. Inter. Ed.* **2011,** *50* (35), 8067-8071.
23. Liang, W.; Carraro, F.; Solomon, M. B.; Bell, S. G.; Amenitsch, H.; Sumby, C. J.; White, N. G.; Falcaro, P.; Doonan, C. J., Enzyme Encapsulation in a Porous Hydrogen-Bonded Organic Framework. *J. Am. Chem. Soc.* **2019,** *141* (36), 14298-14305.
24. Liang, K.; Ricco, R.; Doherty, C. M.; Styles, M. J.; Bell, S.; Kirby, N.; Mudie, S.; Haylock, D.; Hill, A. J.; Doonan, C. J.; Falcaro, P., Biomimetic Mineralization of Metal-Organic Frameworks as Protective Coatings for Biomacromolecules. *Nat. Commun.* **2015,** *6*, 7240.
25. Liang, K.; Coghlan, C. J.; Bell, S. G.; Doonan, C.; Falcaro, P., Enzyme Encapsulation in Zeolitic Imidazolate Frameworks: A Comparison between Controlled Co-Precipitation and Biomimetic Mineralisation. *Chem. Commun.* **2015,** *52* (3), 473-476.
26. Li, Z.; Xia, H.; Li, S.; Pang, J.; Zhu, W.; Jiang, Y., In Situ Hybridization of Enzymes and their Metal–Organic Framework Analogues with Enhanced Activity and Stability by Biomimetic Mineralisation. *Nanoscale* **2017,** *9* (40), 15298-15302.
27. Chui, S. S. Y.; Lo, S. M. F.; Charmant, J. P. H.; Orpen, A. G.; Williams, I. D., A Chemically Functionalizable Nanoporous Material [Cu3(TMA)2(H2O)3]n. *Science* **1999,** *283* (5405), 1148-1150.
28. Lü, X.-F.; Feng, C.-Y.; Li, S.; Liu, G.-H.; Yang, Z., Tyrosinase@HKUST-1: A Super Stable Biocatalyst Efficient for Catecholic Product Synthesis. *Bioresour. Bioprocess.* **2021,** *8* (1), 108.
29. Zhang, R.; Wang, L.; Han, J.; Wu, J.; Li, C.; Ni, L.; Wang, Y., Improving Laccase Activity and Stability by HKUST-1 with Cofactor via One-Pot Encapsulation and Its Application for Degradation of Bisphenol A. *J. Hazard. Mater.* **2020,** *383*, 121130.

30. Pan, Y.; Li, H.; Farmakes, J.; Xiao, F.; Chen, B.; Ma, S.; Yang, Z., How Do Enzymes Orient on Metal-Organic Framework (MOF) Surfaces? *J. Am. Chem. Soc.* **2018,** *140*, 16032-16036.
31. Pan, Y.; Li, Q.; Li, H.; Farmakes, J.; Ugrinov, A.; Zhu, X.; Lai, Z.; Chen, B.; Yang, Z., A General Ca-MOM Platform with Enhanced Acid/Base Stability for Enzyme Biocatalysis. *Chem Catalysis* **2021,** *1*, 146-161.
32. Pan, Y.; Li, H.; Lenertz, M.; Han, Y.; Ugrinov, A.; Kilin, D.; Chen, B.; Yang, Z., One-pot Synthesis of Enzyme@Metal-Organic Materials (MOM) Biocomposites for Enzyme Biocatalysis. *Green Chem.* **2021,** *33*, 4466-4476.
33. Farmakes, J.; Schuster, I.; Overby, A.; Alhalhooly, L.; Lenertz, M.; Li, Q.; Ugrinov, A.; Choi, Y.; Pan, Y.; Yang, Z., Enzyme Immobilization on Graphene Oxide (GO) Surface via One-Pot Synthesis of GO/Metal-Organic Framework Composites for Large-Substrate Biocatalysis *ACS Appl. Mater. Interfaces* **2020,** *12* (20), 23119-23126.
34. Neupane, S.; Patnode, K.; Li, H.; Baryeh, K.; Liu, G.; Hu, J.; Chen, B.; Pan, Y.; Yang, Z., Enhancing Enzyme Immobilization on Carbon Nanotubes via Metal-Organic Frameworks for Large-Substrate Biocatalysis. *ACS Appl. Mater. Interfaces* **2019,** *11* (12), 12133-12141.
35. Jordahl, D.; Armstrong, Z.; Li, Q.; Gao, R.; Liu, W.; Johnson, K.; Brown, W.; Scheiwiller, A.; Feng, L.; Ugrinov, A.; Mao, H.; Chen, B.; Quadir, M.; Pan, Y.; Li, H.; Yang, Z., Expanding the Library of Metal-Organic Frameworks (MOFs) for Enzyme Biomineralization. *ACS Appl. Mater. Interfaces* **2022,** *14* (46), 51619-51629.
36. Pan, Y.; Li, H.; Li, Q.; Lenertz, M.; Zhu, X.; Chen, B.; Yang, Z., Site-Directed Spin Labeling-Electron Paramagnetic Resonance Spectroscopy in Biocatalysis: Enzyme Orientation and Dynamics in Nanoscale Confinement. *Chem Catal.* **2021,** *1*, 207-231.
37. Pan, Y.; Li, H.; Li, Q.; Lenertz, M.; Schuster, I.; Jordahl, D.; Zhu, X.; Chen, B.; Yang, Z., Protocol for Resolving Enzyme Orientation and Dynamics in Advanced Porous Materials via SDSL-EPR *STAR Protoc.* **2021,** *2* (3), 100676.
38. Hubbell, W. L.; López, C. J.; Altenbach, C.; Yang, Z., Technological Advances in Site-Directed Spin Labeling of Proteins. *Curr. Opin. Struct. Biol.* **2013,** *23* (5), 725-733.
39. Cafiso, D. S., Identifying and Quantitating Conformational Exchange in Membrane Proteins Using Site-Directed Spin Labeling. *Acc. Chem. Res.* **2014,** *47* (10), 3102-3109.
40. Fanucci, G. E.; Cafiso, D. S., Recent Advances and Applications of Site-Directed Spin Labeling. *Curr. Opin. Struct. Biol.* **2006,** *16* (5), 644-653.
41. Schiemann, O.; Heubach, C. A.; Abdullin, D.; Ackermann, K.; Azarkh, M.; Bagryanskaya, E. G.; Drescher, M.; Endeward, B.; Freed, J. H.; Galazzo, L.; Goldfarb, D.; Hett, T.; Esteban Hofer, L.; Fábregas Ibáñez, L.; Hustedt, E. J.; Kucher, S.; Kuprov, I.; Lovett, J. E.; Meyer, A.; Ruthstein, S.; Saxena, S.; Stoll, S.; Timmel, C. R.; Di Valentin, M.; McHaourab, H. S.; Prisner, T. F.; Bode, B. E.; Bordignon, E.; Bennati, M.; Jeschke, G., Benchmark Test and Guidelines for DEER/PELDOR Experiments on Nitroxide-Labeled Biomolecules. *J. Am. Chem. Soc.* **2021,** *143* (43), 17875-17890.
42. Evans, E. G. B.; Morgan, J. L. W.; DiMaio, F.; Zagotta, W. N.; Stoll, S., Allosteric Conformational Change of A Cyclic Nucleotide-Gated Ion Channel Revealed by DEER Spectroscopy. *Proc. Natl. Acad. Sci.* **2020,** *117* (20), 10839-10847.
43. Hubbell, W. L.; Gross, A.; Langen, R.; Lietzow, M. A., Recent Advances in Site-Directed Spin Labeling of Proteins. *Curr. Opin. Struct. Biol.* **1998,** *8* (5), 649-656.
44. Hubbell, W. L.; Cafiso, D. S.; Altenbach, C., Identifying Conformational Changes with Site-Directed Spin Labeling. *Nat. Struct. Biol.* **2000,** *7*, 735 - 739.

45. Pan, Y.; Li, Q.; Li, H.; Lenertz, M.; Jordahl, D.; Armstrong, Z.; Chen, B.; Yang, Z., Maximizing the Applicability of Continuous Wave (CW) Electron Paramagnetic Resonance (EPR): What More Can We Do After A Century? *J. Magn. Reson. Open* **2022,** *10-11*, 100060.
46. Lin, R.-B.; Li, L.; Zhou, H.-L.; Wu, H.; He, C.; Li, S.; Krishna, R.; Li, J.; Zhou, W.; Chen, B., Molecular Sieving of Ethylene From Ethane Using A Rigid Metal-Organic Framework. *Nat. Mater.* **2018,** *17* (12), 1128-1133.
47. Chen, X.; Plonka, A. M.; Banerjee, D.; Krishna, R.; Schaef, H. T.; Ghose, S.; Thallapally, P. K.; Parise, J. B., Direct Observation of Xe and Kr Adsorption in a Xe-Selective Microporous Metal-Organic Framework. *J. Am. Chem. Soc.* **2015,** *137* (22), 7007-7010.
48. Yang, J.; Trickett, C. A.; Alahmadi, S. B.; Alshammari, A. S.; Yaghi, O. M., Calcium l-Lactate Frameworks as Naturally Degradable Carriers for Pesticides. *J. Am. Chem. Soc.* **2017,** *139* (24), 8118-8121.
49. Banerjee, D.; Simon, C. M.; Plonka, A. M.; Motkuri, R. K.; Liu, J.; Chen, X.; Smit, B.; Parise, J. B.; Haranczyk, M.; Thallapally, P. K., Metal-Organic Framework with Optimally Selective Xenon Adsorption and Separation. *Nat. Commun.* **2016,** *7* (1), ncomms11831.
50. Sumida, K.; Hu, M.; Furukawa, S.; Kitagawa, S., Structuralization of Ca2+-Based Metal-Organic Frameworks Prepared via Coordination Replication of Calcium Carbonate. *Inorg. Chem.* **2016,** *55* (7), 3700-3705.
51. Mazaj, M.; Mali, G.; Rangus, M.; Žunkovič, E.; Kaučič, V. e.; Zabukovec Logar, N. a., Spectroscopic Studies of Structural Dynamics Induced by Heating and Hydration: A Case of Calcium-Terephthalate Metal-Organic Framework. *J. Phys. Chem. C* **2013,** *117* (15), 7552-7564.
52. Miller, S. R.; Alvarez, E.; Fradcourt, L.; Devic, T.; Wuttke, S.; Wheatley, P. S.; Steunou, N.; Bonhomme, C.; Gervais, C.; Laurencin, D.; Morris, R. E.; Vimont, A.; Daturi, M.; Horcajada, P.; Serre, C., A Rare Example of A Porous Ca-MOF for the Controlled Release of Biologically Active NO. *Chem. Commun.* **2013,** *49* (71), 7773-7775.
53. Chipman, D. M.; Sharon, N., Mechanism of Lysozyme Action. *Science* **1969,** *165* (3892), 454-465.
54. Faber, H. R.; Matthews, B. W., A Mutant T4 Lysozyme Displays Five Different Crystal Conformations. *Nature* **1990,** *348*, 263-266.
55. Bennett, T. D.; Cheetham, A. K., Amorphous Metal–Organic Frameworks. *Acc. Chem. Res.* **2014,** *47* (5), 1555-1562.
56. Ashworth, C., Characterizing Amorphous MOFs. *Nat. Rev. Chem.* **2021,** *5* (5), 298-298.
57. Fonseca, J.; Gong, T.; Jiao, L.; Jiang, H.-L., Metal–Organic Frameworks (MOFs) Beyond Crystallinity: Amorphous Mofs, MOF Liquids And MOF Glasses. *J. Mater. Chem. A* **2021,** *9* (17), 10562-10611.
58. Wu, X.; Yue, H.; Zhang, Y.; Gao, X.; Li, X.; Wang, L.; Cao, Y.; Hou, M.; An, H.; Zhang, L.; Li, S.; Ma, J.; Lin, H.; Fu, Y.; Gu, H.; Lou, W.; Wei, W.; Zare, R. N.; Ge, J., Packaging and Delivering Enzymes by Amorphous Metal-Organic Frameworks. *Nat. Commun.* **2019,** *10* (1), 5165.
59. Li, Q.; Armstrong, Z.; Ugrinov, A.; Chen, B.; Liu, B.; Li, H.; Pan, Y.; Yang, Z., Metal-Organic Materials Enhance Proteolytic Selectivity, Efficiency, and Reusability of Trypsin: A Time-Resolved Study on Proteolysis. *ACS Appl. Mater. Interfaces* **2022,** *15* (7), 8927-8936.
60. Budil, D. E.; Lee, S.; Saxena, S.; Freed, J. H., Nonlinear-Least-Squares Analysis of Slow-Motion EPR Spectra in One and Two Dimensions Using a Modified Levenberg-Marquardt Algorithm. *J. Magn. Reson. A* **1996,** *120* (2), 155-189.

TOC Figure

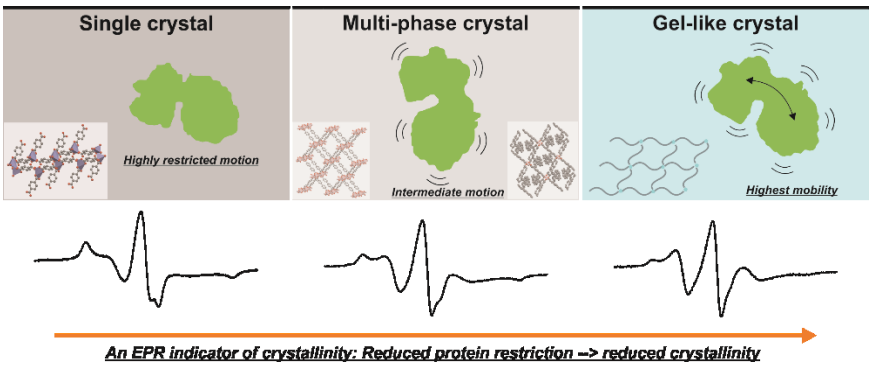
Single crystal
Highly restricted motion
Multi-phase crystal
Intermediate motion
Gel-like crystal
Highest mobility
An EPR indicator of crystallinity: Reduced protein restriction --> reduced crystallinity